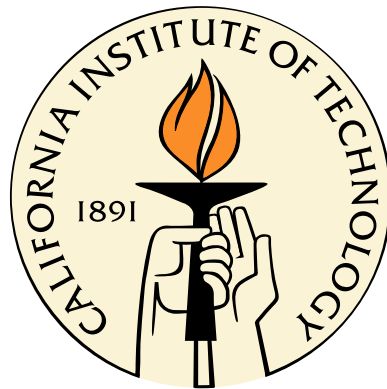


Fluid-structure Interactions of Inverted Leaves and Flags

Thesis by
Boyu Fan

In Partial Fulfillment of the Requirements
for the Degree of
Bachelor of Science



California Institute of Technology
Pasadena, California

2015
(Submitted June 4, 2015)

Acknowledgements

I am most grateful to my advisor, Mory Gharib, for first accepting me into his group almost a year and a half ago and for continually supporting me with his wisdom and kindness. His neverending creativity and enthusiasm has instilled in me a love for fluid mechanics and all of its beautiful mysteries.

I would also like to sincerely thank Julia Cossé, whose mentorship exceeded all expectation. Her patience and astute advice has shaped me into the scientist I am today. I am grateful to John Sader, whose brilliance and energy has been invaluable in my research; to the entire Gharib group, especially Martha Salcedo, Junie Hildebrandt, Chris Roh, and Nathan Martin, for helping me out whenever I needed it; and to Tim Colonius for his feedback and assistance on this thesis, as well as just being an awesome academic advisor.

I am eternally grateful to my loving family and their support in my endeavors.

Last but certainly not least, these last four years at Caltech would not have been the same without all of the cherished friends I have met, to whom words cannot express my love and gratitude. Through all the late nights and sleepy mornings, you all are unforgettable and I certainly could not have made it here without you. I know that Caltech is just the start of our adventures.

This work was supported by the Gordon and Betty Moore Foundation and by the Lester Lees Aeronautics Summer Undergraduate Research Fellowship.

Abstract

Interactions between fluid flows and elastic bodies are ubiquitous in nature. One such phenomena that is encountered on a daily basis is the flapping and fluttering of leaves in the wind. The fluid-structure interaction that governs the physics of a leaf in the wind is poorly understood at best and has potential applications in biomechanics, vehicle design, and energy conversion. We build upon previous work on the flapping dynamics of inverted flags, which are cantilevered elastic sheets with free leading edge and fixed trailing edge that display unique large amplitude oscillatory behaviors. We model a leaf in the laboratory using modified inverted flags, experimentally probing the governing parameters behind leaf fluttering as well as shedding light on the physics behind the inverted flag phenomena. The behavior of these “inverted leaves” studied here display sensitive dependence on two biomechanically relevant parameters, stem-to-leaf rigidity and stem-to-leaf length. In addition, leaves on a tree are not often found alone. We seek to understand the complex interactions of multiple fluttering and flapping leaves by way of examining the interactions between pairs of inverted flags. Coupling through their flow fields, pairs of inverted flags exhibit striking emergent phenomena. We report these observed dynamical behaviors and the conditions upon which they arise.

Contents

Acknowledgements	iii
Abstract	iv
List of Figures	vii
1 Fluid-structure Interactions of Inverted Leaves	1
1.1 Introduction	1
1.1.1 Motivation	1
1.1.2 Plant Morphology	2
1.1.3 Conventional Flag Behavior	3
1.1.4 Inverted Flag Behavior	3
1.2 Methods	4
1.2.1 Experimental Setup	4
1.2.2 Leaf Properties	6
1.2.3 Image Processing & Data Extraction	8
1.3 Results	9
1.3.1 Behavioral Regimes	9
1.3.2 Stem Length & Rigidity Effects	9
1.3.3 Limiting Behavior	10
1.4 Conclusions	13
2 Dynamical Behavior of Coupled Inverted Flags	14
2.1 Introduction	14
2.1.1 Motivation	14
2.1.2 Background	15
2.2 Methods	15
2.3 Results	16
2.3.1 Behavioral Regimes	16

2.3.2 Separation Effects	20
2.4 Conclusions	21
Bibliography	23

List of Figures

1.1	Schematic of inverted flag from side view (left) and top view (right), with major dimensions indicated.	4
1.2	Behavioral regimes of the inverted flag.	5
1.3	Schematic of experimental setup, indicating locations of the flag, clamp, flow direction, and high-speed camera.	5
1.4	Inverted leaf schematic.	6
1.5	Behavioral regimes of the inverted leaf.	7
1.6	Overview of inverted leaf experimental characterization.	7
1.7	Flapping amplitudes of inverted leaves as stem-to-blade length ratio varies.	10
1.8	Flapping amplitudes of inverted leaves as stem-to-blade rigidity ratio varies.	11
2.1	Schematic of coupled inverted flags in a side-by-side configuration.	16
2.3	Stroboscopic progression of coupled flags for varying flow velocities.	18
2.4	Unstable in-phase flapping transitioning to stable out-of-phase flapping.	18
2.5	Erratic flapping of the coupled flags, showing existence of synchronization.	19
2.6	Steady bent state in which both flags remain along the inside, showing synchronization in the semi-constrained flow though the middle (a). Stroboscopic image of the inside-bent state (b).	19
2.7	Out-of-phase collision state. Here, a red “×” indicates that the two flags have collided and one has stopped the other.	20
2.8	Weakly stable in-phase flapping state for low separation.	21
2.9	Transition from unstable in-phase flapping state to an attracting out-of-phase colliding state.	21

Chapter 1

Fluid-structure Interactions of Inverted Leaves

1.1 Introduction

1.1.1 Motivation

In our natural world, interactions between fluid forces and elastic bodies are ubiquitous. Examples can be seen in leaves that flap and flutter in the wind, or fish that bend and deform for propulsion. In living organisms, the prevalence of fluid-structure couplings over rigid body aerodynamics can often lead to unique dynamical behaviors. Thus, the field of bio-inspired engineering has flourished in recent years as researchers seek inspiration from these uniquely natural phenomena. Much work has concentrated on animal locomotion, from the beating of flagella [1], to the jet-propulsion of jellyfish [2, 3], to the paddling propulsion of ducks [4].

However, the fluid-structure interactions of passive organisms, such as the leaves of a plant waving in the wind whose motion require no energy expenditure on account of the plant, has not yet garnered the same attention. From a biological standpoint, the motion of leaves in the wind is important to understand how plants reconfigure their shapes and orientations to reduce drag and mitigate damage in high winds [5, 6] and how mechanical deformation affects photosynthesis and water interception [7]. From an engineering standpoint, the motion of leaves in the wind is important to understand the fundamental physics of fluid-structure interactions, that can then inform research that seeks to reduce vibrational damage to structures and vehicles. It will also inform the design of new systems that harness alternative forms of energy that rely on the capture of fluid kinetic energy [8, 9, 10]. Current horizontal axis wind turbines, the most prevalent method used to capture wind energy, are incredibly large and costly, operating only over a narrow range of wind velocities before damage. Recent work has focused on the possibility of capturing wind energy using the fluttering of flags [11], as well as improving the performance and robustness of vertical axis wind turbines, noted

for their increased power density, by incorporating pliable blades [12].

In order to understand the physics behind the motion of leaves in the wind, one approach is to look towards the widely studied motion of flags in the wind. Experimental studies have made much progress in characterizing the motion of these flags with respect to various parameters [13], as well as visualizing the flow structures [14]. Theoretical studies have focused on computational simulations as well as on the effects of wake structure [15] and stability [16]. Unfortunately, while these flag studies have greatly informed our understanding of the motion of leaves in the wind, they uniformly ignore one crucial parameter: flow orientation. In these studies, flags are defined by a piece of elastic material fixed at the front edge and free at the rear edge, hereby referred to as the “conventional” orientation. Upon observation of the flapping and fluttering of leaves in the wind, it is important to note that there is high variability in wind direction and speed. Thus, using only a conventional flag to model the behavior of a leaf would ignore the majority of the physical states of the system! As the wind may blow in any direction, some leaves in tree are bound to be in an inverted orientation to the wind, with a free front edge and fixed rear edge.

In 2013, Kim et al. was the first to investigate the behavior of a so-called “inverted” flag, with a clamped trailing edge and free leading edge . The result was surprising, to say the least. The inverted flag displays a self-excited large-amplitude flapping motion about an order of magnitude larger than the fluttering motion of conventional flags. A few studies in the literature had observed similar fluttering behaviors in reversed flow orientations, such as the dynamical behavior of cylinders clamped at the rear edge and free at the front edge [18], and the clapping pages of a book orientated with pages pointing into the flow [19]. However, the observation of a large amplitude motion found in inverted flags was unprecedented.

While the inverted flag model captures the effects of flow orientation, another crucial element is required in order to accurately model a leaf: the leaf stem. The experiments presented here build upon the inverted flag model of Kim et al. (2013) by freeing the boundary condition on the rear edge of the sheet and instead, introducing a thin elastic stem fixed at the rear end. This will be henceforth referred to in this study as an inverted leaf. By probing the effects of various parameters on the behavior of these inverted leaves, we aim to understand the morphology of leaves from a fluid mechanical standpoint.

1.1.2 Plant Morphology

Many studies have been conducted assessing the effects of fluid forces on plants. In increasingly high winds and in a conventional orientation, leaves such as that of tulip poplars and red maple, among a great many others, reconfigure by rolling up into a cone, resulting in a drag that grows much slower than the classic U^2 law [5]. In addition, the shape of the base of the leaf blade, where it meets with the leaf stem, was found to contribute to this roll-up [20].

The mechanical properties of the leaf blade and stem are crucial to a plant’s resilience to being blown over or uprooted. Perennial plants such as trees, which take many years to reach sexual maturity, often develop structures to enable them to survive an extreme range of environmental conditions. For trees in high wind, local failure (losing leaves and branches) rather than global failure (uprooting) may be an indication of fit design. The loss of easily replaced features such as leaves and branches, the largest source of drag in a tree, reduces the drag of the tree and decreases the chance of being uprooted, ensuring that the tree will survive.

One important parameter in plant morphology that has received attention is flexural rigidity, or resistance to bending which is dependent on both material (Young’s modulus) and geometric properties (second moment of area). One study found that loblolly pines subjected to higher winds typically had higher flexural rigidities but lower Young’s modulus [21], and while its results are contested and certainly inconclusive [22], it highlights the relevance of wind on plant morphology.

1.1.3 Conventional Flag Behavior

In a uniform flow and neglecting three-dimensional effects, conventional flags typically exhibit three distinct dynamical states: a stretched straight state, a fluttering state, and an aperiodic flutter state [14, 15, 23]. The stretched straight state is characterized by a lack of motion and occurs either below a critical flow velocity or under a critical flag length. In the fluttering state, the motion of the flag consists of traveling waves that move down the length of the flag. The maximum tip amplitude of flutter in the conventional flag never exceeds approximately 0.5 of the flag length [14].

1.1.4 Inverted Flag Behavior

A schematic of the typical inverted flag is presented in Figure 1.1. The motion of inverted flags can be divided into three main behavioral regimes, however, with drastically different properties than the conventional flag [17]. At low wind speeds, only a straight mode with low amplitude flutter is observed (left-most panel in Figure 1.2). Past a certain critical wind speed, U_{lower} , the flag enters a limit-cycle flapping mode with large amplitude periodic flapping (center three panels in Figure 1.2). Past another critical wind speed, U_{upper} , the flag enters a deflected or bent mode also with low amplitude flutter (right-most panel in Figure 1.2). While the fluttering of conventional flags consists of traveling waves that move down the length of the flag, the flapping of the inverted flag is observed to be a stationary wave [17].

Previously, our group at Caltech studied the effect of two non-dimensional parameters that characterize the interaction between fluid flow and elastic sheets [17]. These two parameters, κ and mass ratio μ , represent the ratio of hydrodynamic pressure to elastic restoring forces and the ratio

of fluid-to-solid inertia, respectively. They are defined as

$$\kappa \equiv \frac{\rho U^2 L^3}{D}, \quad \mu \equiv \frac{\rho L}{\rho_s h}$$

where U is the wind velocity, L is the sheet length, h is the sheet thickness, ρ is the fluid density, and ρ_s is the sheet density. The flexural rigidity D of the elastic sheet is defined by $D \equiv Eh^3/[12(1-\nu^2)]$, where E and ν are the Young's modulus and Poisson's ratio of the sheet, respectively. The range of large-amplitude flapping of the inverted flag was found to appear in a narrow range of κ (a function of U), above a certain aspect ratio, and be largely independent of μ .

1.2 Methods

1.2.1 Experimental Setup

Experiments were conducted in an open-loop wind tunnel with a square cross section of side length 1.2 m and capable of producing free-stream velocities between 1.8 and 8.2 m/s (Figure 1.3). The tunnel is composed of an array of 10 x 10 computer fans [24]. The trailing edge of the leaves are clamped vertically between two aluminum strips. Thicknesses of the strips were chosen to balance the trade-off between rigidity and potential effects on the flow structure. For this study, the clamp chosen measured 1.27 cm wide normal to the flow and 1.27 cm in long in the direction of the flow. We assumed and verified that for leaves of lengths much greater than that of the clamp, the effects of the clamp on behavior are negligible.

Images of the leaf motion are captured with a Integrated Design Tools, Inc. NanoSense MkIII high-speed camera mounted above the test section. Images were taken at a frame rate of 100 frames per second, for varying periods of time to capture various dynamical behaviors.

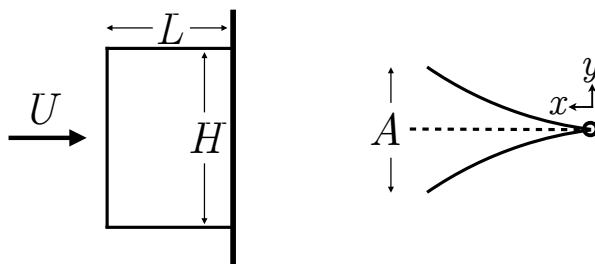


Figure 1.1: Schematic of inverted flag from side view (left) and top view (right), with major dimensions indicated.

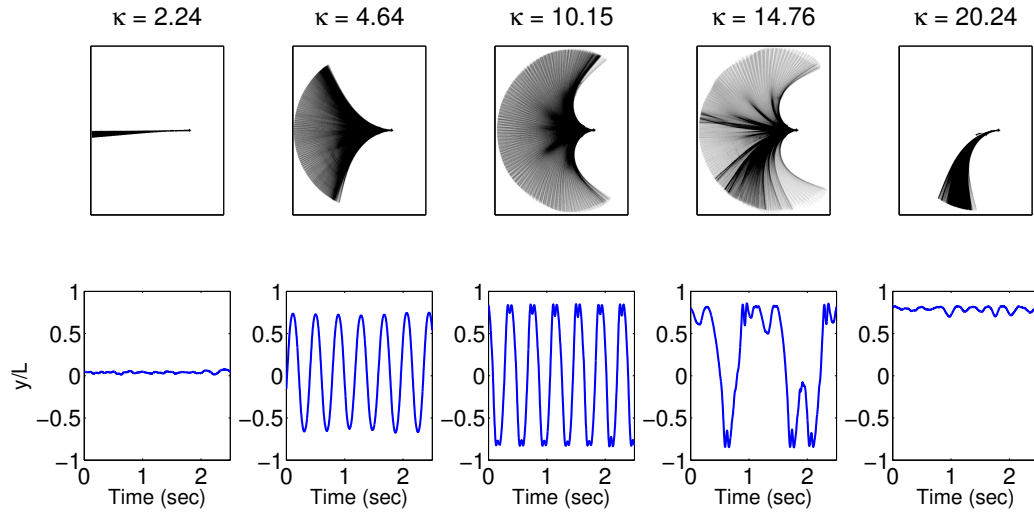


Figure 1.2: Stroboscopic images (upper panels) and corresponding time series (lower panels) of an inverted flag in an increasingly faster free-stream. Images were taken over 2.5 seconds for each panel and overlaid, with darker areas indicating longer flag presence. From left to right as free-stream velocity increases (increasing κ): straight mode (no flapping), flapping mode, flapping mode (larger A), flapping mode (erratic), deflected mode.

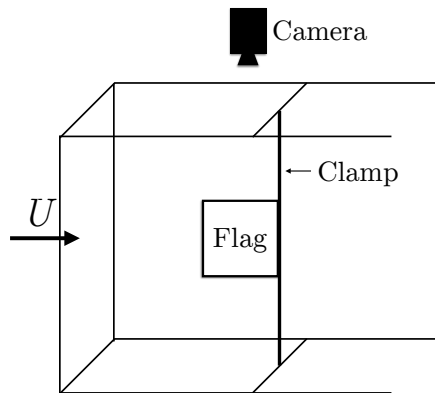


Figure 1.3: Schematic of experimental setup, indicating locations of the flag, clamp, flow direction, and high-speed camera.

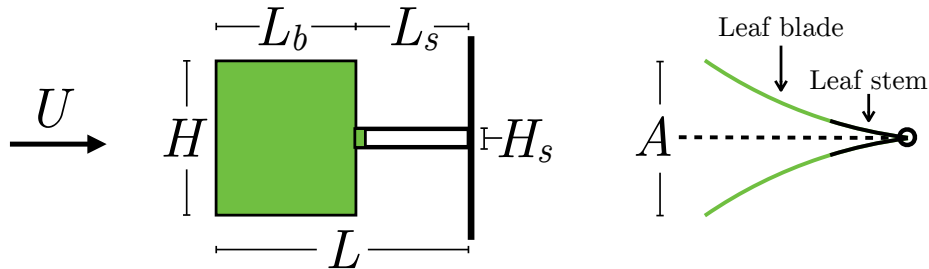


Figure 1.4: Schematic of inverted leaf a from side view (left) and top view (right). Both leaf stem and blade are polycarbonate.

1.2.2 Leaf Properties

To experimentally model the fluid-structure interactions of a leaf, we construct artificial leaves out of polycarbonate, with Young's modulus $E = 2.41 \times 10^9 \text{ N/m}^2$, Poisson's ratio $\nu = 0.38$, and density $\rho_s = 1.2 \times 10^3 \text{ kg/m}^3$. As depicted in Figure 1.4, the leaf blades in this study are constructed from single rectangular sheets, of varying lengths L_b , constant height $H = 17.78 \text{ cm}$, and constant thickness $h_b = 0.0508 \text{ cm}$, along with a small rectangular tab jutting from one edge, of height constant $H_s = 1.27 \text{ cm}$ equal to that of the stem and constant length 1.27 cm . This small rectangular tab is used to join the blade to the stem, constructed from two slender rectangular bars that are sandwiched together along with the leaf blade tab and joined with cyanoacrylate adhesive (Superglue). These two joined slender rectangular bars form the leaf stem, of varying lengths L_s , constant height $H_s = 1.27 \text{ cm}$, and varying total thickness h_s . Note that the total length of the leaf will be denoted L with no subscript, to remain consistent with the notation for traditional inverted flags with no stem and fully fixed rear edge.

The rationale behind the two-layer composite design of the leaf stem was to maintain as much simplicity and isotropy in the leaf as possible. Because of their observed regular oscillatory flapping motions, we aimed for symmetry, resulting in the stem-leaf blade tab-stem composite. The leaf blade tab used to join the stem and blade was designed to be as short as possible while maintaining a solid connection between the two regions of the leaf. Therefore, we ignore any effects of either the leaf blade tab or the two-layer composite nature of the stem and assume that they are negligible. Further consideration of these effects and other leaf designs are beyond the scope of this thesis and can be a avenue for future work.

We assume that fluid loading on the stem itself is negligible compared to the elastic forces in the stem because of its small surface area. This was confirmed by placing the stem by itself in the wind tunnel without a blade, where no motion was observed for any wind velocity. We have chosen to focus our attention on the presence of the stem in shedding light on the behavior of leaves in nature. We have also chosen to fix the overall lengths of all leaves/flags studied to $L = 17.78 \text{ cm}$, in order to fix the Reynolds number, $\text{Re} \equiv UL/\nu = O(10^4)$, where ν is the kinematic viscosity of air. In this

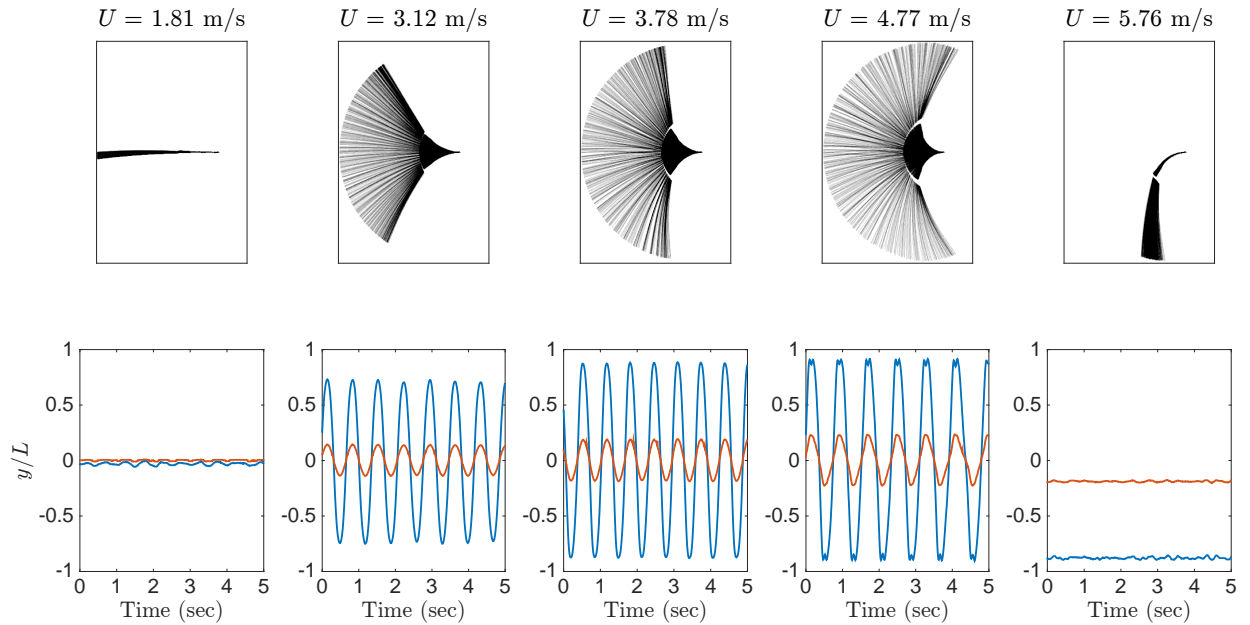


Figure 1.5: Stroboscopic images (upper panels) and corresponding time series (lower panels) of an inverted leaf in an increasingly faster free-stream. Overlaid images were taken over 5 seconds. The leaf blade and stem can clearly be distinguished in the stroboscopic view. In the times series, the blue curves corresponds to the tip positions of the full leaf at the end of the blade, while the orange curves corresponds to the positions of the end of the stem, where it meets the blade.

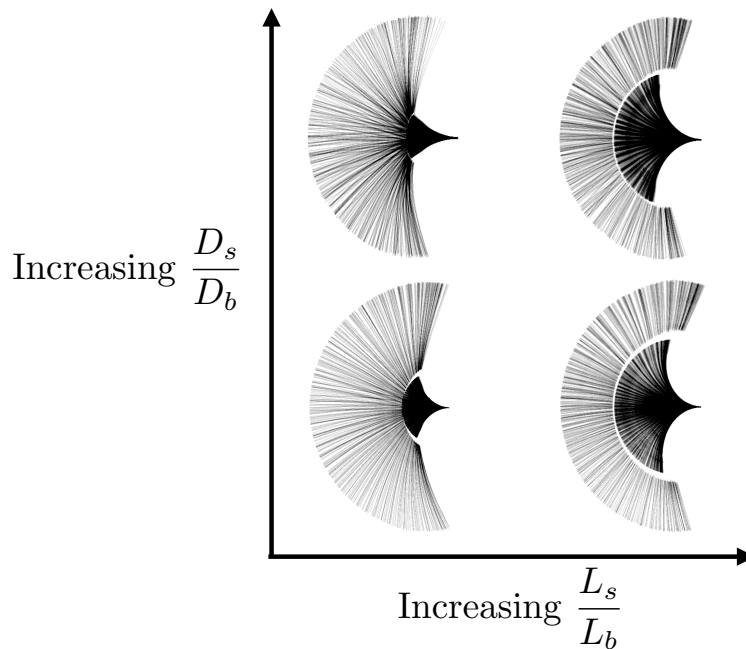


Figure 1.6: Overview of leaf experimental characterization, indicating the two parameters of interest: stem-to-leaf rigidity and stem-to-leaf length. Stroboscopic images featured here display inverted leaves at various wind speeds that correspond to each's respective maximum flapping amplitude.

thesis, we will be considering the effects of both stem length and stem rigidity on the behavior and dynamics of our inverted leaves (see Figure 1.6). We examine stem-to-blade length ratio L_s/L_b of 5/9 and 9/5 (henceforth referred to as the “low” and “high” stem-to-blade length ratio, respectively) by varying the lengths of the stem and blade accordingly such that overall length L is constant. We then examine stem-to-blade flexural rigidity ratio D_s/D_b of 3.38 and 8, (henceforth referred to as the “low” and “high” stem-to-blade rigidity ratio, respectively) by only varying the thicknesses of the leaf stem and keeping the leaf blade rigidity constant. Note that because blade and stem are constructed from the same material, $D_s/D_b = h_s^3/h_b^3$.

1.2.3 Image Processing & Data Extraction

The top edge of the inverted leaf is painted with white correction fluid for increased contrast with a black background during image capture. Images of the top edge of the leaves are then processed using MATLAB. Edge detection is used in order to extract the leaf position. Various behavioral features, such as amplitude and frequency can thus be measured. Stroboscopic images of the leaf motion are generated by overlaying all images taken over the sample period using transparency. Darker areas will indicate increased presence in that location during its flapping cycle, allowing us to precisely see when flapping is periodic versus erratic.

Both the top edge of the stem and the top edge of the blade are tracked through high-speed photography, with the key points of interest being the location of the tip of the blade and the location of the tip of the stem where at the stem-blade joint. Because the top edge of the blade is tracked rather than the centerline of the blade, slight three-dimensional effects can be seen as a result of the slight three-dimensional bending at the top and bottom edge of the blade when under high fluid loading. Since we have kept H constant, three-dimensional effects increase with greater L_s/L_b , as the aspect ratio of the blade increases. These effects can be observed in the stroboscopic images presented (see Figures 1.6, 1.5), manifested by the slightly greater range of motion of the leaf blade in the deflected position. However, because all three-dimensional effects in the leaves studied are small relative to the extraordinarily dramatic large-amplitude behavior of the inverted configuration, we will assume that these three-dimensional effects have negligible effects on the general behaviors and trends observed.

In order to mollify error introduced by the composite structure as well as other experimental error, three of each leaf/flag tested in this thesis were constructed and results are averaged between the three. Again, relative to the highly regular large-amplitude dynamical behavior of the inverted configuration, experimental error was found to have negligible effects on the general behaviors and trends observed.

1.3 Results

1.3.1 Behavioral Regimes

The presence of the leaf stem in the inverted leaf does not preclude any of the major behavioral regimes observed in the inverted flag. As flow velocity increases, the inverted leaf exhibits a straight mode, regular flapping mode followed by brief erratic flapping, and a deflected mode. Figure 1.5 presents stroboscopic images and time series of stem and blade tip positions for the same inverted leaf at select flow velocities. The time series of stem and blade tip positions are normalized by the full length of the leaf, L . Similar to the inverted flag, the full leaf amplitude (blade tip) increases with flow velocity in the flapping regime. We observe that the stem tip amplitude also increases with flow velocity and is always exactly in-phase with the blade tip. This supports the notion that the oscillations of the inverted leaf form a stationary wave, just as in the inverted flag, rather than a travelling wave as in the conventional flag.

Rather than the curved mode shape of the flapping inverted flag, which is similar to the fundamental mode of the linearized Euler-Bernoulli beam [17], the flapping inverted leaf exhibits a starkly different shape. The stem bends with a curved shape, but the blade remains almost perfectly straight at all flow velocities (see stroboscopic images in Figures 1.6, 1.5 and compare with inverted flag images in Figure 1.2). Because of the change in rigidity and sharp corner at the narrow joint between the stem and blade, all the strain in the blade from fluid loading is concentrated at the stem-blade joint. The high stress concentrations located around the joint will be further discussed in a later section on the limiting behavior of inverted leaves.

1.3.2 Stem Length & Rigidity Effects

As stem-to-blade length ratio increases, the flapping regime shifts to higher flow velocities as both U_{lower} and U_{upper} increase (see Figure 1.7). This trend persists regardless of the stem-to-blade rigidity ratio, although for more rigid stems during the transition from flapping to bent, this upward shift is much more pronounced. Similarly, as stem-to-blade rigidity ratio increases, the flapping regime shifts to higher flow velocities (see Figure 1.8) and this trend persists regardless of the stem-to-blade length ratio.

Overall, the leaf with the highest velocity flapping regime is also the leaf with the widest flapping range ($\Delta U = U_{upper} - U_{lower}$): the leaf with the shorter and more rigid stem. Compared with the behavior of the inverted flag (with the entire rear edge fixed but same full length L , height H , and blade thickness), this leaf also happens to be the leaf that most closely resembles the inverted flag in both flapping regime (see Figure 1.7b) as well as shape. These results suggests that the presence of the stem serves to decrease the threshold flow velocities for flapping and bent regimes.

The maximum full leaf flapping amplitudes show a high monotonic dependence on stem rigidity

and low dependence on stem length. For the low rigidity stems (see Figure 1.7a), maximum flapping amplitude is greater than that of the inverted flag and closer to the maximum possible normalized amplitude of 2. As stem rigidity increases, maximum flapping amplitude decreases. For a perfectly stiff stem, the maximum possible flapping amplitude is only $2L_b/L$, which decreases as stem length increases. Behavior at this limit will be discussed in further detail in the following section.

The stem flapping amplitudes prescribe to the exact same behavioral regimes as the full leaf behavior for all leaves. Interestingly, the stem amplitudes do not appear to level off and plateau at the end of the flapping regime quite as much as the full leaf amplitudes. Rather, they monotonically increase up until the immediate transition into the bent regime. However, whereas inverted flags and the full leaves typically reach normalized amplitudes of about 1.8 to 1.9 before transitioning to the bent regime, the tip amplitudes never exceed 1.5. At low stem lengths, the rigidity dependence of stem amplitude is dramatic (see Figure 1.8a) as highly rigid stems flap very little. At high stem lengths, this dependence is much less significant (see Figure 1.8b) as the stem amplitudes are comparable throughout the flapping regime.

1.3.3 Limiting Behavior

Next, we consider the limits at very high stem rigidity, and then at vanishing stem length. Figure 1.9 presents the case where $D_s/D_b = 27$. At some critical flow velocity within the flapping regime, the stress concentration at the blade-stem joint causes the polycarbonate to fail and crack at the joint. This failure occurred repeatedly at $U = 5.1$ m/s for all three leaves constructed. Once the blade-

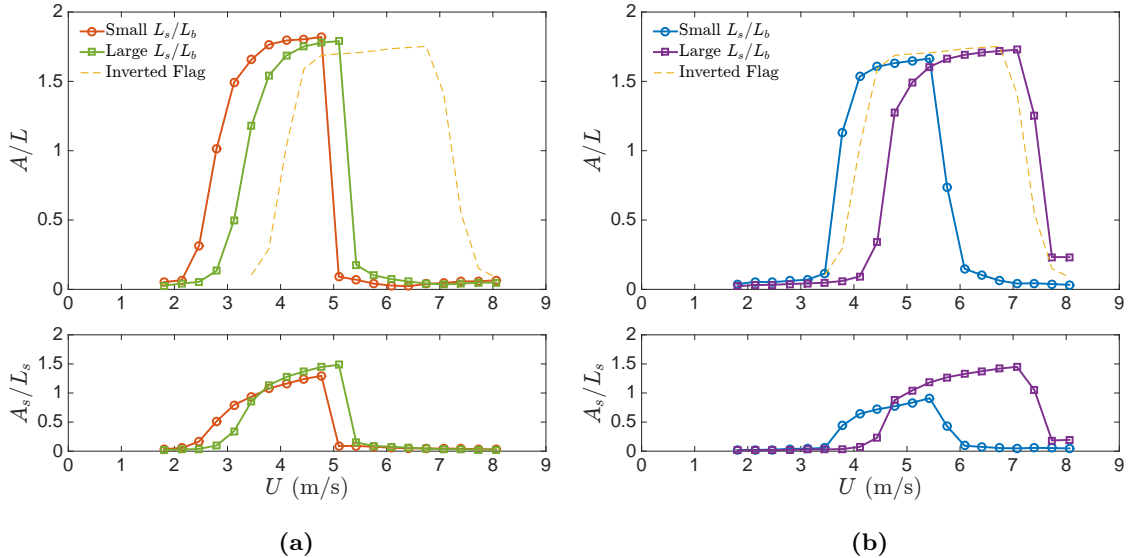


Figure 1.7: Full leaf (top) and stem (bottom) flapping amplitudes of inverted leaves as stem-to-blade length ratio varies. Stem length effects are shown for both (a) low stem rigidity leaves as well as (b) high stem rigidity leaves.

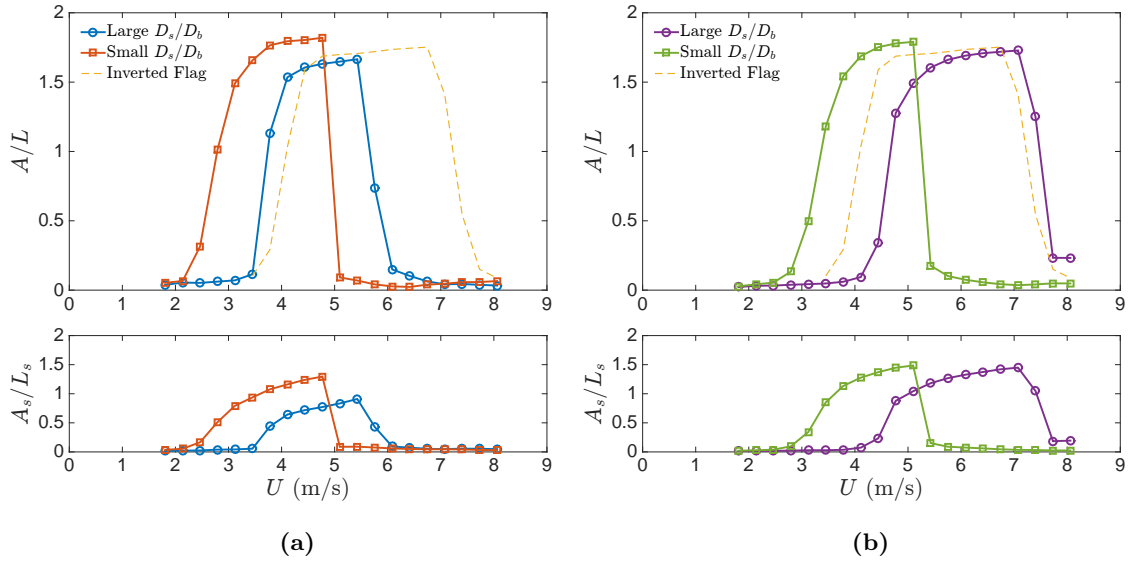


Figure 1.8: Full leaf (top) and stem (bottom) flapping amplitudes of inverted leaves as stem-to-blade rigidity ratio varies. Stem rigidity effects are shown for both (a) low stem length leaves as well as (b) high stem length leaves.

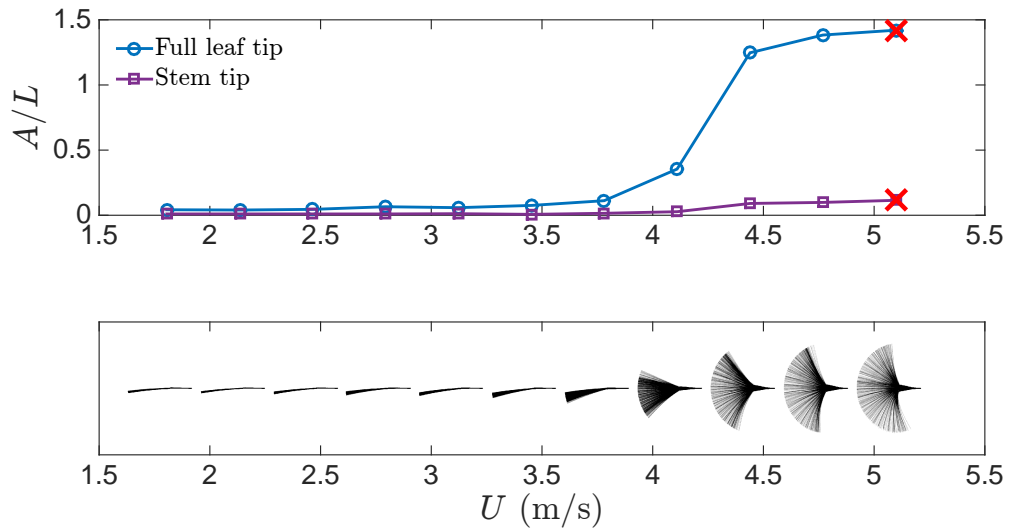


Figure 1.9: High stem-to-blade rigidity limit, indicating wind velocity at which leaf breakage occurs.

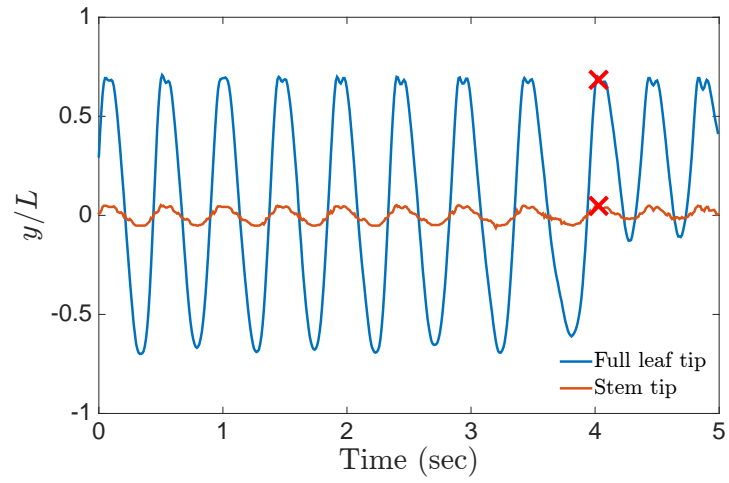


Figure 1.10: Time series of the high stem-to-blade rigidity limiting case at the wind velocity at which leaf breakage occurs.

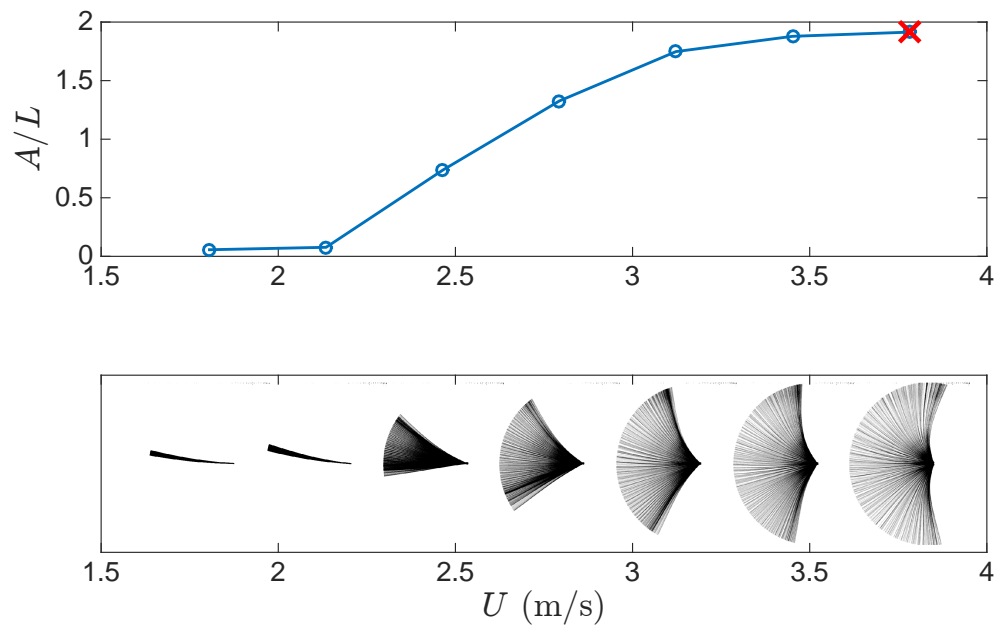


Figure 1.11: Low stem-to-blade length limit, indicating wind velocity at which leaf breakage occurs.

stem joint cracks, the leaf immediately transitions to the bent regime (see Figure 1.10). Similarly, in the vanishing stem limit, the polycarbonate also fails at the leaf blade-stem joint after a critical flow velocity ($U = 3.8$ m/s) within the flapping regime (see Figure 1.11). While the model leaves in this study are only crude approximations of the diverse range of leaf morphologies found in nature, this limiting behavior lends insight to the importance of stem rigidity and stem length on leaf behavior, as well as to the adaptations in leaf morphology of plants that thrive in high wind conditions in order to avoid damage.

1.4 Conclusions

The dynamics of the inverted leaf are found to heavily depend on stem length and stem rigidity. Not only do the critical threshold velocities for flapping shift accordingly, but also the amplitude of motion, stem curvature, and conditions for failure. Future avenues for work can potentially lie in comparing these experimental results with wind tunnel testing of real tree leaves, similar to Vogel (1989), but rather in an inverted configuration. In addition, flow visualization would be extremely useful in revealing the underlying vortex dynamics.

Chapter 2

Dynamical Behavior of Coupled Inverted Flags

2.1 Introduction

2.1.1 Motivation

In the previous chapter, we experimentally studied the fluid-structure interactions of a single leaf in an inverted orientation. However, upon observation of the fluttering of a real leaf on a real tree, one may notice that this leaf is rarely alone. Rather, each leaf interacts and couples with the multitude of leaves in close proximity. Thus, in order to understand the physics behind leaf fluttering, we must uncover the dynamical interactions between multiple elastic structures and their flow fields.

The fluid mechanics of multiple bodies is a topic of great interest, having been applied to fish to understand schooling patterns and animal locomotion [25], as well as humans to decrease drag during swimming competitions [26]. It is also a topic of immediate relevance. In the field of renewable energy, for example, one method of increasing the viability of wind farms is through studying the interactions between multiple wind turbines to determine optimal spacing and maximize power density [27].

From a fundamental standpoint, the interactions between flexible structures are still very poorly understood. The complexities of the fluid-structure coupling and the multiple body coupling compound one another. The majority of work in the subject thus far has focused on extending our knowledge of the archetypal conventional flag model by considering interactions between multiple conventional flags [14, 28, 29, 30, 31, 32]. However, as seen in a recent study of an inverted flag, flow orientation drastically changes the fundamental nature of the fluid-structure interaction [17]. How then, does flow orientation change the fundamental nature of coupled flags? What sorts of emergent behavior are produced? In this chapter, we aim to extend our limited understanding of coupled fluid-structure interactions by examining pairs of inverted, rather than conventional, flags.

Here, we present results from experiments on side-by-side inverted flags. These results are not only of fundamental importance, but also directly inform future structural and vehicular design.

2.1.2 Background

Relevant background on single inverted flags was given in the previous chapter and will not be repeated here. As for coupled conventional flags, recent experimental and theoretical studies have analyzed the coupling between two-dimensional conventional flags and observed unique behavior and synchronization. For a constant flow velocity, Zhang et al. (2000) experimentally observed the existence of various cooperative dynamical modes in pairs of side-by-side 2D flags: locked in-phase flapping for low inter-flag separation, out-of-phase flapping for higher inter-flag separation, and decreasing interaction strength as inter-flag separation increases further. This is qualitatively similar to the findings of studies on the synchronized wakes of fixed side-by-side cylinders in which symmetric out-of-phase wakes are more frequently observed for larger separations [33].

2.2 Methods

Experiments were conducted in the same open-loop wind tunnel as in the previous chapter, with a square cross section of side length 1.2 m and capable of producing free-stream velocities between 1.8 and 8.2 m/s. Two inverted flags were placed side-by-side in the tunnel, as depicted in Figure 2.1. The trailing edge of each flag was clamped vertically between two aluminum strips each measuring 1.27 cm wide. Both flags are polycarbonate and identical to the control inverted flag discussed in the previous chapter, with length $L = 17.78$ cm, height $H = 17.78$ cm, and thickness $h_b = 0.0508$ cm. Images of the flag motion were captured with a Integrated Design Tools, Inc. NanoSense MkIII high-speed camera mounted above the test section. The camera's field-of-view was sufficiently large to capture the full range of motion of both flags in a single image, obviating the need for two cameras and synchronized triggering. Images were taken at a frame rate of 100 frames per second and we track the positions of both flag tips simultaneously over a period of 5 to 20 sec.

Behaviors at various flow velocities are observed for two different trailing edge separation widths: $d/L = 1.86$ at which flags could never collide at any point in range of motion, and $d/L = 1.14$ where flags could collide and were indeed observed to collide. Both flags point directly into the flow with negligible angle-of-attack. We denote the phase difference between the two flags' oscillation cycles as ϕ , where one period corresponds to a flag starting from one flapping extrema and returning to the same flapping extrema.

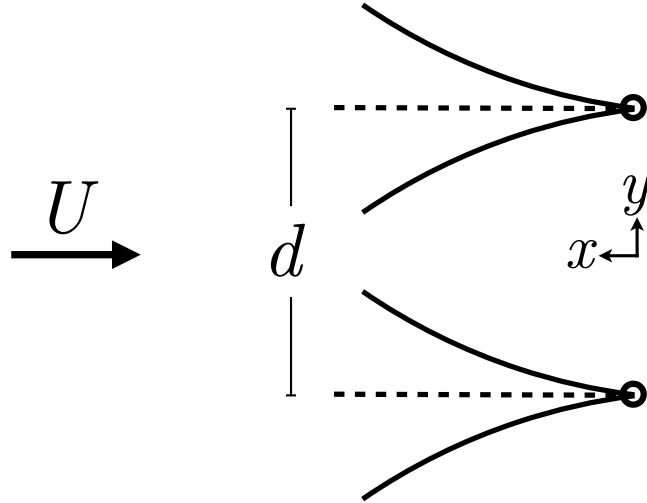


Figure 2.1: Schematic of coupled inverted flags in a side-by-side configuration.

2.3 Results

2.3.1 Behavioral Regimes

First, consider when nondimensional separation width is large enough such that the inverted flags never collide. This was found experimentally to approximately occur at $d/L = 1.86$. The three main behavioral regimes of straight, flapping, and bent persist in the coupled flag system. While flapping onset for the coupled flag system does not significantly deviate from the single flag case, transition from flapping to bent occurs at lower flow velocities in the coupled flag system.

New dynamical subregimes are observed corresponding to various flow velocities and Figure 2.2 depicts a summary of the steady state behaviors observed in each flow velocity regime. First, beginning in the top row of Figure 2.2, the straight mode at low flow velocities ($0 < U < 3.9$ m/s) exhibits little synchronization as the separation between the flags is large compared to the small-scale flutter observed in the flags.

Immediately at the critical flow velocity for flapping and continuing into the low velocity regions of the flapping regime ($3.9 < U < 4.9$ m/s), the only steady state observed is an attracting out-of-phase ($\phi = \pi$) flapping state. Systems initialized with in-phase ($\phi = 0$) initial conditions and various staggered phase ($0 < \phi < \pi$) initial conditions all rapidly destabilize and converge to the out-of-phase flapping state. Figure 2.4 presents a times series of the flag tip positions at $U = 4.8$ m/s initialized in an in-phase flapping state. The in-phase state rapidly destabilizes and transitions to an out-of-phase state over the course of 4 sec.

In the out-of-phase flapping state, tip angular displacement for both flags is greater in the inside semi-confined region between the clamps than in the outside region (see Figure 2.3). This persists

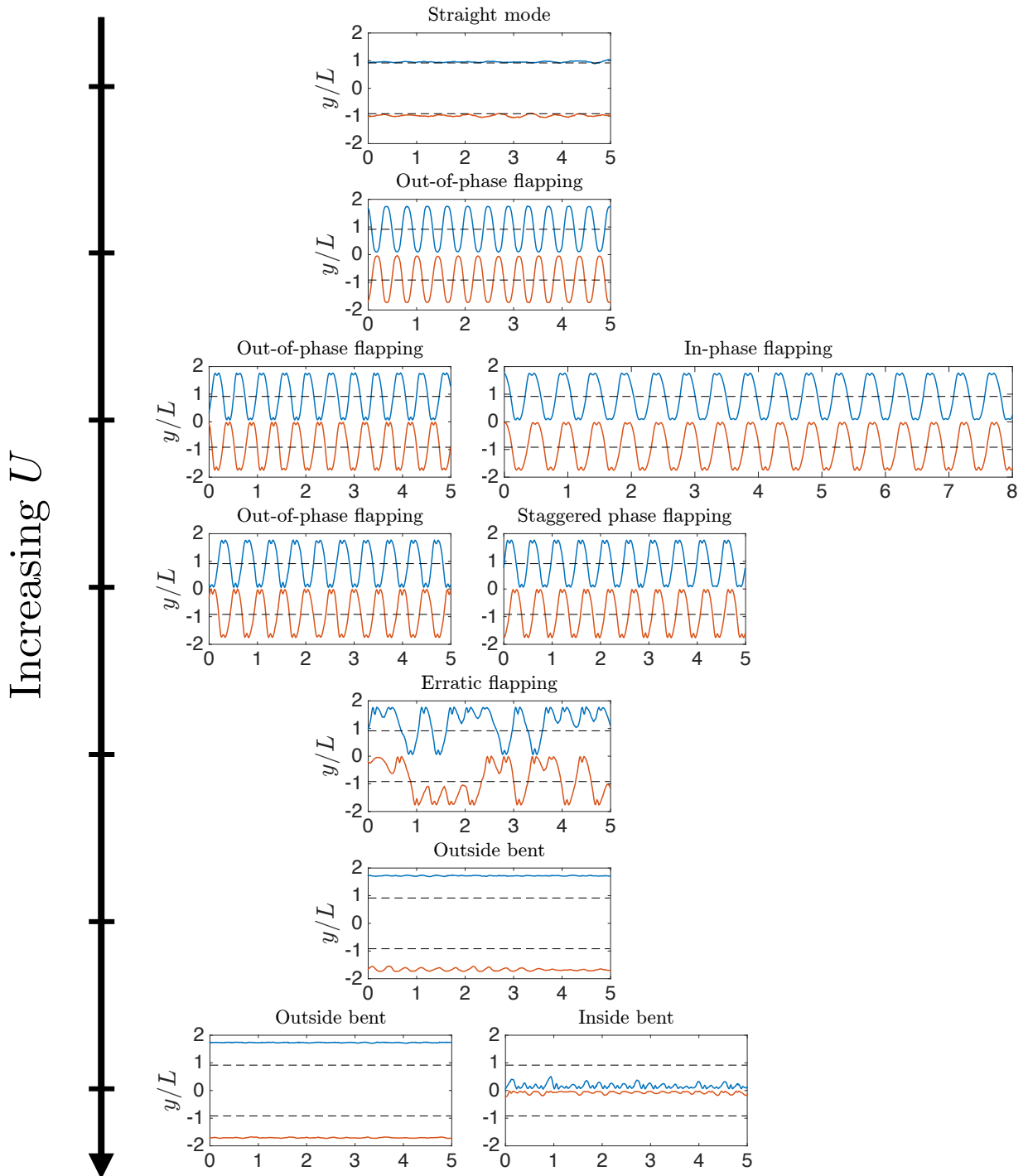


Figure 2.2: Steady states of the coupled flag system for varying flow velocities for $d/L = 1.86$.

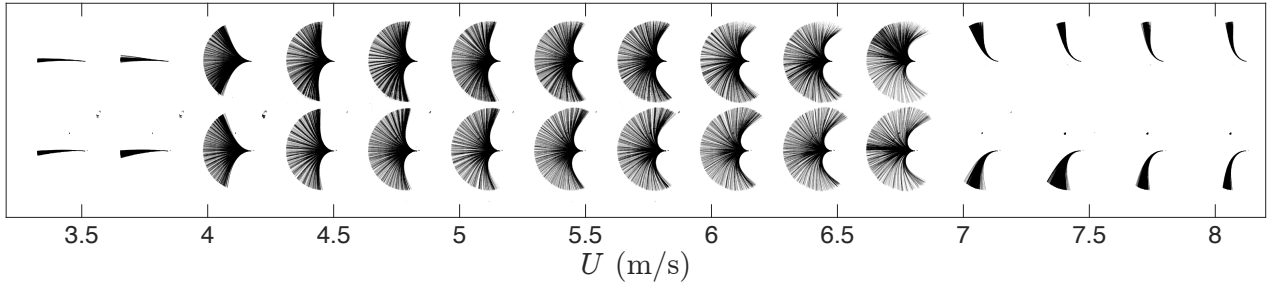


Figure 2.3: Stroboscopic progression of coupled flags for varying flow velocities. Note that not all possible states at each flow velocity are depicted. All flapping states depict out-of-phase flapping. All bent states depict outside-bent states.

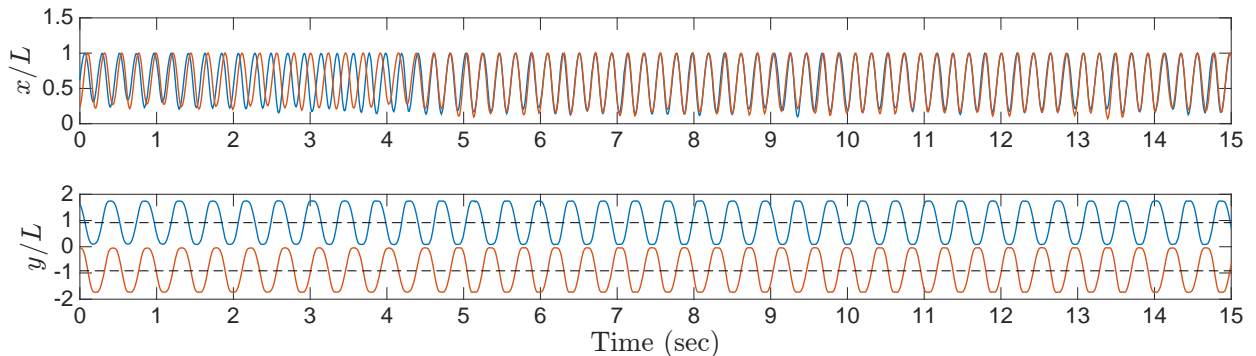


Figure 2.4: Unstable in-phase flapping transitioning to stable out-of-phase flapping.

through all out-of-phase flapping modes at all flow velocities.

Next, at higher flow velocities ($4.9 < U < 5.9$ m/s), the coupled flag system exhibits both steady out-of-phase and in-phase flapping states, depending on initial conditions. The out-of-phase state remains highly attracting as before, but this new stable in-phase state is extremely sensitive to initial conditions and perturbations in the flow field. Staggered phase flapping states quickly destabilize into the out-of-phase flapping state.

In the next behavioral regime ($5.9 < U < 6.3$ m/s), steady out-of-phase, in-phase, and staggered phase flapping states all emerge, depending on initial conditions.

Next ($6.3 < U < 6.9$ m/s), the coupled flags enter an erratic flapping state (see Figure 2.5). However, while the flags jump from side to side in a seemingly erratic fashion, the shedding of vortices still appears to occasionally synchronize. This synchronization appears to be most prominent when both flags bend into the region between the two flags, i.e. along the inside of the clamps (fixed trailing edges). In this region, the behavior of the coupled flags is most akin to the out-of-phase flapping state, where the flags phase lock and appear to “clap” in the confined space.

When the coupled flags first enter the bent regime ($6.9 < U < 7.9$ m/s), they preferentially bend towards the outside of the center region, i.e. away from each other. If initialized with both flags on

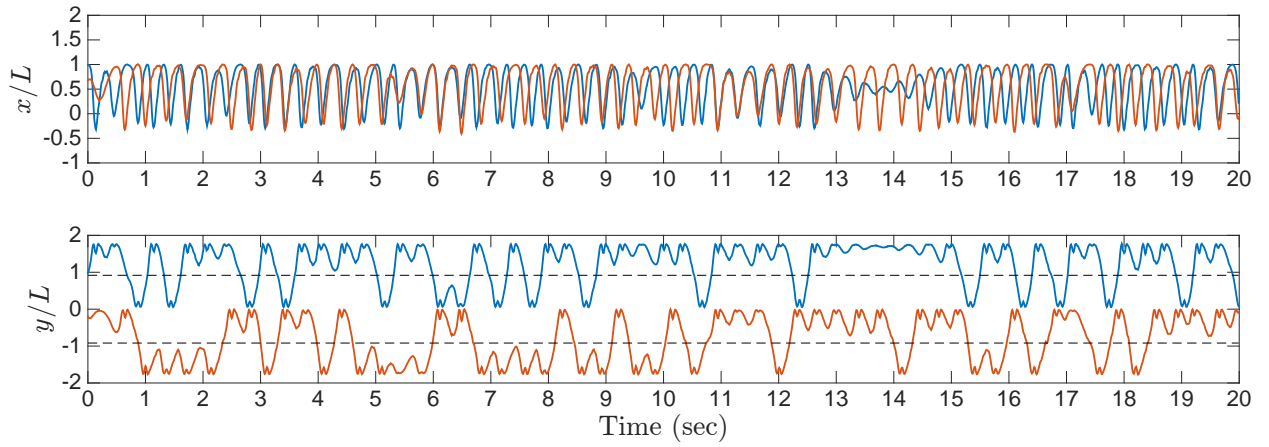
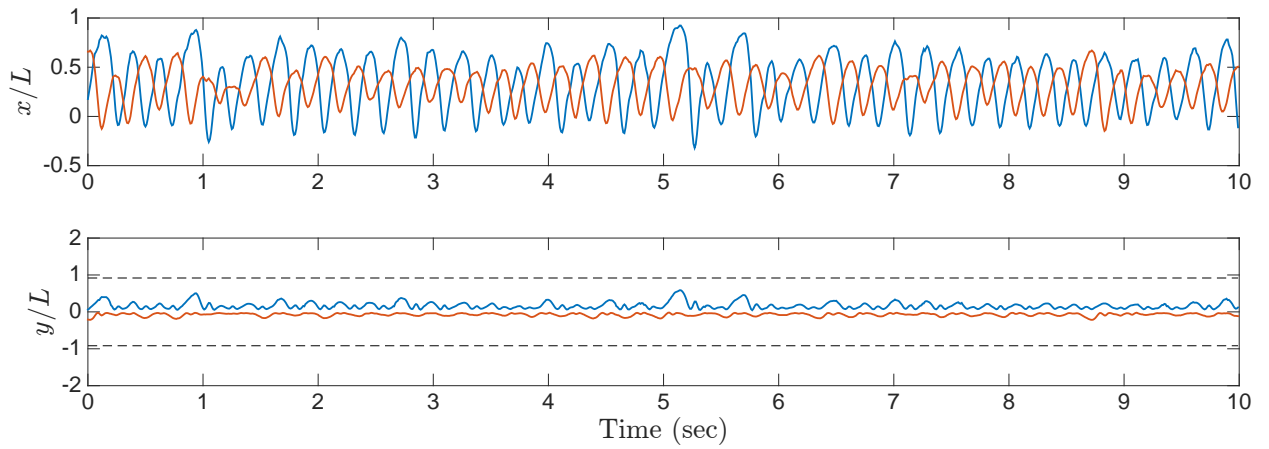
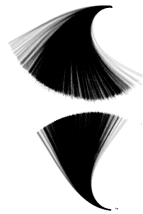


Figure 2.5: Erratic flapping of the coupled flags, showing existence of synchronization.



(a)



(b)

Figure 2.6: Steady bent state in which both flags remain along the inside, showing synchronization in the semi-constrained flow through the middle (a). Stroboscopic image of the inside-bent state (b).

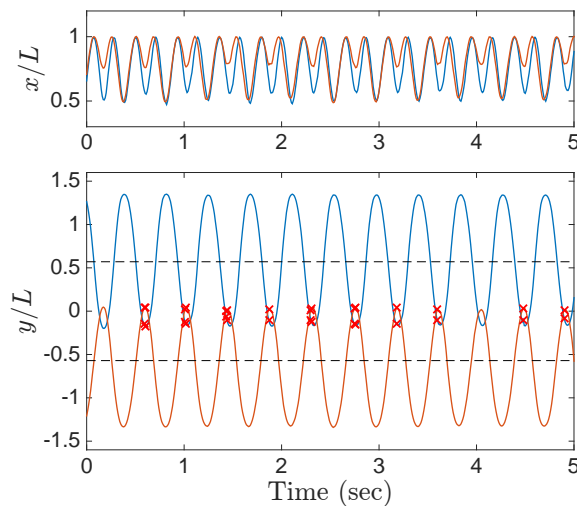


Figure 2.7: Out-of-phase collision state. Here, a red “×” indicates that the two flags have collided and one has stopped the other.

the inside, the system rapidly transitions to the preferential outside-bent configuration. For the case when one flag bends inward and the other bends outward, the inward bending flag switches and the system still stabilizes to the preferential outside-bent configuration.

Finally, for higher flow velocities ($U > 7.9$ m/s), both inside-bent and outside-bent configurations are possible. In the inside-bent state (see Figure 2.6), the flags synchronize in an alternating behavior, rather than the “clapping” behavior seen frequently at other flow regimes.

2.3.2 Separation Effects

When separation is decreased such that flag collision is possible ($d/L = 1.14$), an out-of-phase colliding state dominates the dynamics of the system (see Figure 2.7). In the lower velocity regions of the flapping regime, this attracting out-of phase state is the only steady state observed. Various initial phase conditions all transitioned to this “clapping” state.

At higher flow velocities in the middle of the flapping range, a steady in-phase flapping state emerges in addition to the out-of-phase “clapping” state. In this locked in-phase state, the system corrects for small perturbations/irregularities in the flow (see Figure 2.8 during $3 < t < 5$ sec). However, sufficiently large perturbations push the system back into the “clapping” state.

At sufficiently high flow velocities towards the end of the flapping regime, the steady in-phase flapping state observed at lower velocities is no longer present. However, it is difficult to determine whether this is simply a result of larger flow irregularities that serve to destabilize in-phase flapping towards the more energetically favorable out-of-phase clapping state. Under initially in-phase flapping conditions (see Figure 2.9), the transition from in-phase to out-of-phase is an extremely

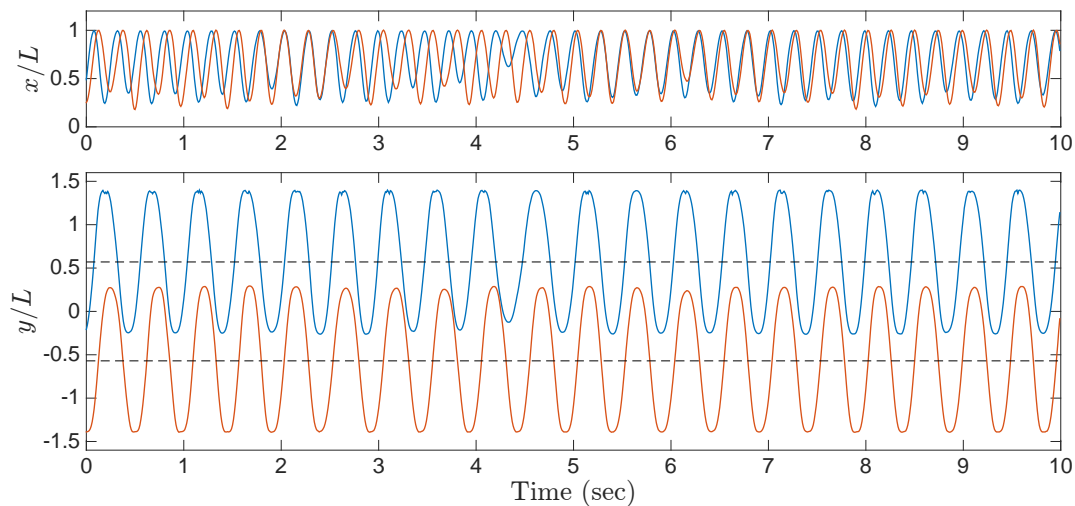


Figure 2.8: Weakly stable in-phase flapping state for low separation.

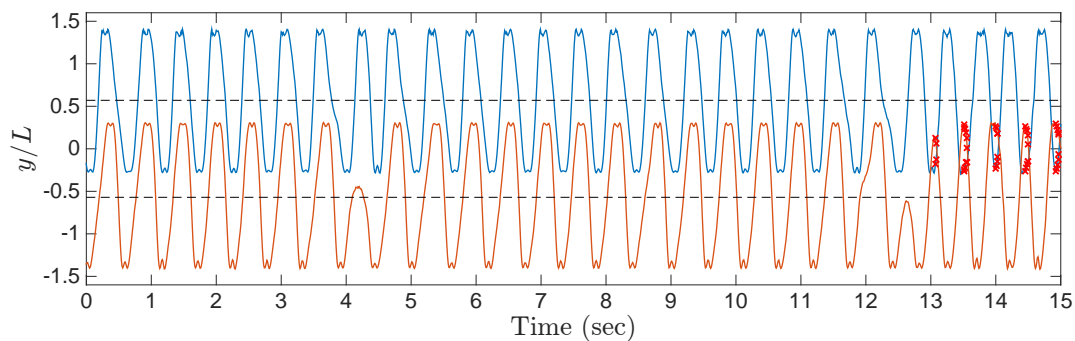


Figure 2.9: Transition from unstable in-phase flapping state to an attracting out-of-phase colliding state.

abrupt transition rather than a smooth gradual transition. At these high velocities, there is a strong restoring response to flow irregularities that are insufficiently large (e.g. at $t = 4.2$ sec), and we observe dramatic instances where one flag is stopped mid-flap by the other flag's shed vortex.

In the bent regime, the coupled flags universally favor the outside-bent configuration. The semi-confined region in between the two flags is heavily disfavored as the low separation distance prevents the flags from reaching a fully bent configuration in the inside region.

2.4 Conclusions

The dynamics of the side-by-side coupled flag system are shown to exhibit emergent behaviors that are strongly dependent on flow velocity. As opposed to the single flag system, coupled flags display similar flapping onset velocities, but lower flapping-to-bent critical transition velocities. In addition,

the dominant mode of flapping is universally the out-of-phase flapping mode. For sufficiently large separations such that flags never collide, in-phase flapping and staggered phase flapping grow in stability as flow velocity increases. When flags undergo erratic flapping, synchronization of vortex shedding persists. In the bent regime, outside-bent configurations are always stable, while inside-bent configurations become stable past a critical flow velocity. For small separations such that flags collide with each other, the out-of-phase flapping mode results in a clapping behavior. Staggered phase flapping modes disappear, leaving only a very weakly stable in-phase flapping mode that is observed at sufficiently high flow velocities.

One crucial avenue for future work is in flow visualization, which would reveal deeper insights into the vortex dynamics that underlay the phenomena presented. While only side-by-side coupled inverted flags were presented in this thesis, it is reasonable to expect synchronization to occur in tandem inverted flags (one flag in front and one flag behind), as well as in end-on-end coupled inverted flags (one flag above and one flag below). These configurations present other avenues for future work.

Bibliography

- [1] R. Dreyfus, J. Baudry, M. L. Roper, M. Fermigier, H. A. Stone, and J. Bibette, “Microscopic artificial swimmers,” *Nature*, vol. 437, pp. 862–865, 10 2005.
- [2] J. O. Dabiri, S. P. Colin, J. H. Costello, and M. Gharib, “Flow patterns generated by oblate medusan jellyfish: field measurements and laboratory analyses,” *The Journal of Experimental Biology*, vol. 208, pp. 1257–1265, 4 2005.
- [3] J. C. Nawroth, H. Lee, A. W. Feinberg, C. M. Ripplinger, M. L. McCain, A. Grosberg, J. O. Dabiri, and K. K. Parker, “A tissue-engineered jellyfish with biomimetic propulsion,” *Nature Biotechnology*, vol. 30, pp. 792–797, 08 2012.
- [4] D. Kim and M. Gharib, “Characteristics of vortex formation and thrust performance in drag-based paddling propulsion,” *Journal of Experimental Biology*, vol. 214, pp. 2283–2291, 7 2011.
- [5] S. Vogel, “Drag and reconfiguration of broad leaves in high winds,” *Journal of Experimental Botany*, vol. 40, pp. 941–948, 08 1989.
- [6] S. A. Etnier and S. Vogel, “Reorientation of daffodil (narcissus: Amaryllidaceae) flowers in wind: drag reduction and torsional flexibility,” *American Journal of Botany*, vol. 87, pp. 29–32, 1 2000.
- [7] L. Tadrist, M. Soudreau, and E. de Langre, “Wind and gravity mechanical effects on leaf inclination angles,” *Journal of Theoretical Biology*, vol. 341, pp. 9–16, 1 2014.
- [8] G. W. Taylor, J. R. Burns, S. A. Kammann, W. B. Powers, and T. R. Welsh, “The energy harvesting eel: a small subsurface ocean/river power generator,” *IEEE Journal of Oceanic Engineering*, vol. 26, pp. 539–547, 10 2001.
- [9] L. Tang, M. P. Païdoussis, and J. Jiang, “Cantilevered flexible plates in axial flow: Energy transfer and the concept of flutter-mill,” *Journal of Sound and Vibration*, vol. 326, pp. 263–276, 9 2009.

- [10] K. Singh, S. Michelin, and E. de Langre, “The effect of non-uniform damping on flutter in axial flow and energy-harvesting strategies,” *Proceedings of the Royal Society of London A*, vol. 468, pp. 3620–3635, 09 2012.
- [11] Y. Xia, S. Michelin, and O. Doaré, “Fluid-solid-electric lock-in of energy-harvesting piezoelectric flags,” *Physical Review Applied*, vol. 3, p. 014009, Jan 2015.
- [12] J. Cossé, *On the behavior of pliable plate dynamics in wind : application to vertical axis wind turbines*. PhD thesis, California Institute of Technology, 5 2014.
- [13] S. Taneda, “Waving motions of flags,” *Journal of the Physical Society of Japan*, vol. 24, p. 392, 2 1968.
- [14] J. Zhang, S. Childress, A. Libchaber, and M. Shelley, “Flexible filaments in a flowing soap film as a model for one-dimensional flags in a two-dimensional wind,” *Nature*, vol. 408, pp. 835–839, 12 2000.
- [15] B. S. H. Connell and D. K. P. Yue, “Flapping dynamics of a flag in a uniform stream,” *Journal of Fluid Mechanics*, vol. 581, pp. 33–67, 6 2007.
- [16] S. Alben and M. J. Shelley, “Flapping states of a flag in an inviscid fluid: Bistability and the transition to chaos,” *Physical Review Letters*, vol. 100, p. 074301, 2 2008.
- [17] D. Kim, J. Cossé, C. Huertas Cerdeira, and M. Gharib, “Flapping dynamics of an inverted flag,” *Journal of Fluid Mechanics*, vol. 736, 12 2013.
- [18] S. Rinaldi and M. P. Païdoussis, “Theory and experiments on the dynamics of a free-clamped cylinder in confined axial air-flow,” *Journal of Fluids and Structures*, vol. 28, pp. 167–179, 1 2012.
- [19] P. Buchak, C. Eloy, and P. M. Reis, “The clapping book: Wind-driven oscillations in a stack of elastic sheets,” *Physical Review Letters*, vol. 105, p. 194301, 11 2010.
- [20] S. Vogel, *The Life of a Leaf*. The University of Chicago Press, 2012.
- [21] F. W. Telewski and M. J. Jaffe, “Thigmomorphogenesis: Anatomical, morphological and mechanical analysis of genetically different sibs of *Pinus taeda* in response to mechanical perturbation,” *Physiologia Plantarum*, vol. 66, pp. 219–226, 4 1986.
- [22] S. Vogel, *Life’s Devices*. Princeton University Press, 1988.
- [23] M. J. Shelley and J. Zhang, “Flapping and bending bodies interacting with fluid flows,” *Annual Review of Fluid Mechanics*, vol. 43, pp. 449–465, 1 2011.

- [24] E. Johnson and J. Jacob, *Development and Testing of a Gust and Shear Wind Tunnel for NAVs and MAVs*. American Institute of Aeronautics and Astronautics, 2015/01/30 2009.
- [25] D. Weihs, “Hydromechanics of fish schooling,” *Nature*, vol. 241, pp. 290–291, 1 1973.
- [26] A. J. Silva, A. Rouboa, A. Moreira, V. M. Reis, F. Alves, J. P. Vilas-Boas, and D. A. Marinho, “Analysis of drafting effects in swimming using computational fluid dynamics,” *Journal of Sports Science & Medicine*, vol. 7, pp. 60–66, 3 2008.
- [27] J. O. Dabiri, “Potential order-of-magnitude enhancement of wind farm power density via counter-rotating vertical-axis wind turbine arrays,” *Journal of Renewable and Sustainable Energy*, vol. 3, 7 2011.
- [28] L. Ristroph and J. Zhang, “Anomalous hydrodynamic drafting of interacting flapping flags,” *Physical Review Letters*, vol. 101, p. 194502, Nov 2008.
- [29] S. Alben, “Wake-mediated synchronization and drafting in coupled flags,” *Journal of Fluid Mechanics*, vol. 641, pp. 489–496, 12 2009.
- [30] L. Zhu, “Interaction of two tandem deformable bodies in a viscous incompressible flow,” *Journal of Fluid Mechanics*, vol. 635, pp. 455–475, 9 2009.
- [31] S. Kim, W.-X. Huang, and H. J. Sung, “Constructive and destructive interaction modes between two tandem flexible flags in viscous flow,” *Journal of Fluid Mechanics*, vol. 661, pp. 511–521, 10 2010.
- [32] E. Uddin, W.-X. Huang, and H. J. Sung, “Interaction modes of multiple flexible flags in a uniform flow,” *Journal of Fluid Mechanics*, vol. 729, pp. 563–583, 8 2013.
- [33] I. Peschard and P. Le Gal, “Coupled wakes of cylinders,” *Phys. Rev. Lett.*, vol. 77, pp. 3122–3125, 10 1996.